J. Fluid Mech. (1994), *vol.* 274, *pp.* 243–265

The effect of spanwise system rotation on Dean vortices

By O. JOHN E. MATSSON AND P. HENRIK ALFREDSSON

Department of Mechanics/Fluid Physics, Royal Institute of Technology, S-100 44 Stockholm, Sweden

(Received 7 July 1993 and in revised form 14 March 1994)

An experimental study is reported of the flow in a high-aspect-ratio curved air channel with spanwise system rotation, utilizing hot-wire measurements and smoke visualization. The experiments were made at two different Dean numbers (De), approximately 2 and 4.5 times the critical De for which the flow becomes unstable and develops streamwise vortices. For the lower De without system rotation the primary Dean instability appeared as steady longitudinal vortices. It was shown that negative spanwise system rotation, i.e. the Coriolis force counteracts the centrifugal force, could cancel the primary Dean instability and that for high rotation rates it could give rise to vortices on the inner convex channel wall. For positive spanwise system rotation, i.e. when the Coriolis force enhanced the centrifugal force, splitting and merging of vortex pairs were observed. At the higher De secondary instabilities occurred in the form of travelling waves. The effect of spanwise system rotation on the secondary instability was studied and was found to reduce the amplitude of the twisting and undulating motions for low negative rotation. For low positive rotation the amplitude of the secondary instabilities was unaffected for most regions in parameter space.

1. Introduction

Body forces may strongly affect the stability and transition to turbulence of laminar shear flows. Instabilities associated with body forces manifest themselves through the formation of counter-rotating vortices and may appear in many natural and engineering flow situations. Potential sources for such forces are density gradients, streamline curvature and/or system rotation. Examples of fluid machinery where these effects may be important are heat exchanger and turbines.

Linear stability analysis of fluid flows where body forces are the dominant instability factor and the *principle of exchange of stabilities* is valid (i.e. the instability gives rise to a steady flow pattern) usually gives good results with respect to the onset of instability. For curved channel flow the primary instability, in the form of counter-rotating streamwise vortex pairs, appears at a critical Dean number $De_{cr} = 36$ in the narrow-gap approximation ($\gamma \ll 1$), where $De = Re\gamma^{1/2}$, $Re = U_b d/\nu$, $\gamma = d/R$ and U_b is the bulk velocity (i.e. the average velocity across the channel width d). The primary instability can be seen as due to an imbalance between the centrifugal force and the radial pressure gradient.

The Coriolis force can give rise to longitudinal vortices in, for instance, plane channel flow with spanwise system rotation, see Alfredsson & Persson (1989). The Coriolis acceleration is defined as $\boldsymbol{a}_{cor} = 2\boldsymbol{\Omega} \times \boldsymbol{U}$, where $\boldsymbol{\Omega}$ is the system rotation

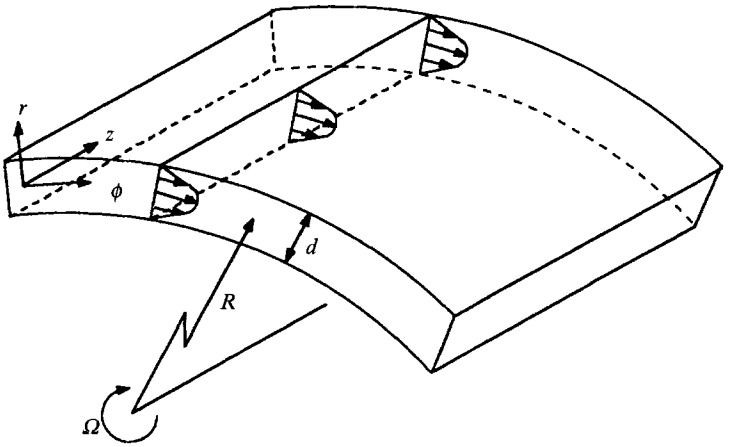

FIGURE 1. Definition of flow geometry in curved channel flow with spanwise system rotation.

vector and $\boldsymbol{U}$ is the velocity vector expressed in the rotating system. The force will be directed in the opposite direction to the acceleration and, depending on the sign of the spanwise rotation component, the force can be directed towards either of the walls. As the base flow is a parabolic velocity profile, there will be an unstable stratification of the Coriolis force on one side of the channel and a stable stratification on the other side, in engineering literature usually denoted as the pressure and suction side, respectively. For viscous channel flow with system rotation the stability is governed by the Reynolds number and a non-dimensional parameter which we call the rotation number defined as $Ro = \Omega d/U_b$. The lowest Reynolds number for which vortices may be amplified is 88.9 and this occurs at a rotation number of 0.5, which can be compared with the critical Reynolds number, $Re_c = 7696$, for which Tollmien–Schlichting waves in plane channel flow without system rotation are amplified.

The combined effects of streamline curvature and system rotation were first studied by Matsson & Alfredsson (1990) in a curved channel with spanwise system rotation, see figure 1. Depending on the direction of the rotation, the Coriolis force will either enhance or counteract the centrifugal force. They solved the viscous linear stability problem for this case and their experiments showed good quantitative correspondence with the theory regarding the rotation rate for which the flow should be stabilized. For certain parameter combinations the *principle of exchange of stabilities* does not hold and Matsson (1993) showed that an instability in the form of travelling, slightly inclined, streamwise-oriented vortices determines the critical Reynolds number. For strong negative rotation the Coriolis force will give rise to vortices on the convex channel wall and for high absolute values of the rotation number ($|Ro| \geqslant 3$) the flow will be stabilized.

The curved rotating channel flow has a counterpart in the Taylor–Dean flow which appears in a partially filled, horizontally oriented Taylor–Couette apparatus, see Mutabazi *et al.* (1988). In that case rotation of the inner cylinder, with the outer one stationary, sets up a velocity profile for which two regions are centrifugally unstable with one region in between which is stable. This will give rise to time-dependent modes of instability which are similar to those in the curved channel with spanwise system rotation, see Mutabazi *et al.* (1989) and Chen & Chang (1992). In contrast to rotating curved channel flow, time-dependent modes have been observed experimentally in Taylor–Dean flow.

The different flow cases mentioned above are all confined flows between rigid boundaries. However, the same effects exist for flows with one free and one rigid boundary. The corresponding flow case for plane channel flow with spanwise system rotation is plane boundary-layer flow with spanwise system rotation. In that case streamwise vortices appear only when the Coriolis force is directed towards the wall (Masuda & Matsubara 1989). Matsubara & Masuda (1990) showed that when the Coriolis force stabilizes the boundary layer it tends to inhibit the spatial growth of turbulent spots. Görtler flow on a concave wall with spanwise system rotation has been analysed with linear stability theory by Aouidef, Wesfreid & Mutabazi (1992) and Zebib & Bottaro (1993). Also for this case stabilization or destabilization of vortices is possible when the Coriolis force counteracts or enhances the centrifugal force, respectively.

1.1. *Curved channel flow*

Earlier experimental and numerical work on curved channel flow has shown that the primary instability may be exposed to several different types of secondary instability. Travelling waves of both long and short wavelength have been observed, as well as a spanwise instability which causes merging and appearance of vortex pairs (sometimes denoted an Eckhaus instability).

The stability analysis of curved channel flow started with Dean (1928), who studied the flow in a curved channel with infinite spanwise aspect ratio as a simplified problem of the flow in a curved pipe. He found theoretically that the motion in a curved channel can become unstable to infinitely small stationary disturbances at $De = 36$. Finlay, Keller & Ferziger (1988) made a numerical simulation of the primary and secondary instability of curved channel flow. In their simulation they used streamwise- and spanwise-periodic boundary conditions which to some extent limit the possible flow behaviour. However, in addition to the primary instability they found two types of travelling waves in the streamwise direction, which they named undulating and twisting motion. The undulating motion is similar to wavy Taylor–Couette vortices and it has a much longer wavelength than the twisting motion which also has a counterpart in Taylor–Couette flow, see Andereck, Dickman & Swinney (1983) and Adereck, Liu & Swinney (1986). Finlay *et al.* suggest that the twisting motion results from the spanwise inflectional profiles of the streamwise velocity and that the undulating motion arises from the curvature of the streamlines in the Dean vortices. Le Cunff & Bottaro (1993) made a linear stability analysis of the spanwise and wall-normal profiles of the streamwise velocity field obtained from numerical simulations and concluded that the twisting motion was due to the spanwise inflectional profile whereas the undulation was of centrifugal origin and related to the wall-normal profile.

Numerical simulations of Dean flow with in- and outflow boundaries together with a large spanwise aspect ratio have been reported by Bottaro, Matsson & Alfredsson (1991), Matsson, Bottaro & Alfredsson (1991) and Bottaro (1993). Such a simulation more closely resembles an experiment than simulations with streamwise-periodic boundary conditions. They found that the primary instability initially grows exponentially in the streamwise direction with a growth rate in agreement with linear theory. Further downstream the disturbance amplitude attained a maximum and decreased to a slightly lower and almost constant level. The larger the Dean number, the nearer to the start of curvature was the amplitude at the maximum level. In these simulations merging and splitting of vortex pairs were also observed for $De/De_{cr} > 2.43$ depending on the inlet conditions.

For curved channels with large aspect ratio the first experiment, to the authors knowledge, was made by Brewster, Grosberg & Nissan (1959) who visualized the flow and verified a critical Dean number of 36. Cheng, Nakayama & Akiyama (1977) investigated the influence of the spanwise aspect ratio on the critical Dean number and found that sidewall effects become important and increase the critical Dean number at a ratio below 8, whereas Finlay & Nandakumar (1990) showed from two-dimensional numerical simulations that the influence of the sidewalls could extend more than 5 channel widths into the channel. Kelleher, Flentie & McKee (1980) made smoke visualizations together with hot-wire measurements of the velocity profile. At a high Dean number, $De/De_{cr} = 7$, these experiments indicated the existence of a secondary instability preceding turbulent flow. Another experiment in the same channel was performed by Ligrani & Niver (1988). They show smoke visualization photographs in a cross-flow plane where Dean vortices appear as a mushroom-shaped pattern. A rocking motion of the mushroom at $De/De_{cr} > 2.5$ was related to the secondary twisting motion. Ligrani *et al.* (1992) show power spectra of the streamwise velocity measured with a hot wire which showed a rather distinct peak which they related to the twisting motion. The frequency of the twisting motion was 0.8 (at $De/De_{cr} = 3.93$) when non-dimensionalized with the channel width and the bulk velocity. They also observed, through smoke visualization, the secondary undulating motion at $1.1 < De/De_{cr} < 3.4$.

Matsson & Alfredsson (1990) carried out flow visualization with suspended reflective flakes in water in a curved channel of high aspect ratio and mapped out various flow regimes as a function of downstream distance and Dean number. At high De they found a secondary instability in the form of short-wavelength travelling waves. Matsson & Alfredsson (1993) showed from measurments in an air channel that the spectrum of the streamwise velocity signal at $De = 4.5De_{cr}$ contains two peaks. Their interpretation was that the low-frequency peak was due to the undulating motion and that the high-frequency peak was related to the twisting motion. By measuring time signals of the streamwise velocity in the cross-flow plane and analysing the spectra by selectively looking at the energy content in narrow frequency bands around the two maxima they were able to plot the physical regions of the instabilities. The twisting motion appears with a maximum in the inflow region between a vortex pair and the undulating motion appears with two maxima near the concave wall. As the twisting motion develops downstream, the disturbance energy integrated over the cross-flow plane behaves in a similar manner to the disturbance amplitude of the primary instability: first an exponential growth followed by a maximum and then the amplitude levels off to an almost constant value. The locus in the maximum of the radial profiles of the twisting disturbance at the inflow region moves towards the concave wall during the growth phase and then remains at a fairly constant radial position. The undulating motion showed two maxima which were positioned symmetrically in the spanwise direction around the inflow region.

Included in the category of secondary instability is a spanwise instability which causes merging and splitting of vortex pairs, see Guo & Finlay (1991). For curved and/or rotating channel flow the stability boundary for spanwise disturbances is a closed loop in the (β, Re)-plane where spanwise wavenumber β is defined as $\beta = 2\pi d/\lambda$, where λ is the spanwise wavelength. This is in contrast to Taylor–Couette flow where the boundary is an open region. Inside the boundary the vortices are stable to spanwise disturbances. However, when the wavenumber is too large, and outside the stability boundary, two vortex pairs will merge into one pair which will cause a smaller wavenumber inside the boundary. Correspondingly, when the wavenumber is

too small, two pairs of vortices will split into three pairs. Guo & Finlay (1994) found that when the primary vortices have a small amplitude, different spanwise wavelengths can occur simultaneously without interactions. Merging and splitting of vortex pairs set in when the primary vortices have reached a nonlinear level. Bottaro (1993) made numerical simulations with both a temporal and a spatial code. In the temporal model (streamwise-periodic boundary conditions) the spanwise secondary instability was time-dependent. However, in the spatial model (inlet-outlet conditions) splitting and merging of vortex pairs was steady. In an experiment non-ideal inlet conditions, such as free-stream unsteadiness or inhomogeneity, will give vortices that either move in the spanwise direction or will be locked. This will cause either time-dependent (Ligrani & Niver 1988) or stationary spanwise secondary instabilities (Matsson & Alfredsson 1992).

Finlay, Guo & Olsen (1993) made spectral element simulations of the steady parabolized Navier–Stokes equations to compare simulated smoke patterns and calculated spatially developing flow. They found that smoke visualizations show a correct picture of the flow only for streamwise-independent curved channel flow and that the spanwise secondary instability may not be properly indicated with smoke.

The transition to turbulent flow in a curved channel has been studied by Bland & Finlay (1991). They simulated the transition in a box with periodic spanwise and streamwise boundary conditions. However, the spanwise box included only one vortex pair which is insufficient in order to study merging and splitting processes which are important for the transition process. Matsson, Bottaro & Alfredsson (1991) studied curved channel flow at $De/De_{cr} = 6.53$ by using numerical simulations of spatially developing flow with inflow-outflow boundaries. A spanwise-periodic flow with an aspect ratio of 9 allowed spanwise interactions of vortex pairs. The numerical simulations seemed to be able to predict the general features of the flow development when compared with hot-wire measurements.

1.2. *Curved channel flow with spanwise system rotation*

As spanwise system rotation is introduced the fluid flow in a curved channel exhibits interesting new flow phenomena, see Matsson & Alfredsson (1990). When the Coriolis force counteracts the centrifugal instability, flow visualization shows at low De a cancellation of the primary instability and at higher De of the secondary twisting instability. Linear stability analysis shows that there is a region in parameter space, in agreement with flow visualization results, where the critical Reynolds number is increased compared to Dean flow without system rotation. In this region of parameter space the *principle of exchange of stabilities* is not valid, see Matsson (1993). Instead, the flow bifurcates to a time-dependent instability where the roll cells move in the spanwise direction with a small streamwise wavenumber.

This paper will focus on hot-wire measurements and smoke visualizations of the primary instability in a curved channel with and without spanwise system rotation. We will also study the effect of spanwise system rotation on the secondary instabilities. The experimental set-up, measuring and flow visualization procedure are presented in § 2. Section 3 shows hot-wire measurements and smoke visualization of the primary instability with and without spanwise system rotation. In § 4 the effects of spanwise system rotation on secondary instabilities are shown through hot-wire measurements and there is discussion of the results in § 5. When spanwise system rotation is present both measurements and visualizations show a dramatic effect on the centrifugal instability in curved channel flow.

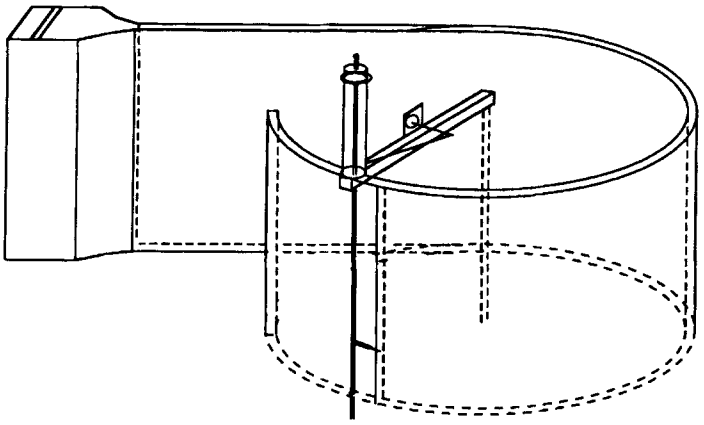

FIGURE 2. View of the experimental air channel.

2. Experimental set-up and procedure

The experimental set-up was basically the same as in the experiment by Matsson & Alfredsson (1992). It consisted of four main parts namely: (1) the stationary air supply system including a fan, flow rate measurement and regulation devices; (2) the rotating table with a rotary coupling for the air supply and slip rings for electrical signals; (3) the flow channel; and (4) the traversing system.

The channel was of open, blowing type. The air supply was a constant-r.p.m. centrifugal fan where the flow rate was adjusted by two mechanical throttles. The flow rate delivered to the channel was measured by the pressure drop over an orifice plate flow meter located in a straight pipe between the fan and the rotating table.

The rotating table had a diameter of 1.2 m. It was driven via a belt from a variable-speed DC-motor with a gear box. The air was fed to the rotating table through a rotating coupling. Electrical signals to the hot wire and the traversing system were given through a high-quality slip ring system which introduced negligible noise to the hot-wire signal.

The channel consisted of the inlet section with stagnation chamber and contraction, followed by a plane channel, 40 channel widths long, after which the curved section of 270° or 180 channel widths followed, see figure 2. The hot wire was calibrated against the parabolic velocity profile at the end of the straight part of the channel. The channel width was 10.5 mm and the radius of curvature at the channel centreline was 400 mm. The spanwise aspect ratio of the channel was choosen as large as 29 in order to have a minimal effect from the sidewalls.

The vortices were artificially triggered by small holes (diameter 1 mm) in the outer wall of the straight channel seven channel widths from the start of curvature. Five holes were symmetrically positioned around the spanwise centreline 15 mm apart in the spanwise direction. Owing to the higher pressure inside the channel there was a slight leakage of air through the holes, enough to generate five pairs of vortices of equal strength at the same spanwise positions as the holes. However, no indication of vortices was observable in the streamwise velocity measured at the start of curvature.

Smoke visualizations were performed by heating two vertically mounted stainless steel wires (diameter 0.08 mm) and continuously dropping paraffin oil along the wires. The wires were located in the middle of the channel at $x/d = 60$. Each wire consisted of a thin stainless steel portion with a length of 100 mm connected at both ends to a

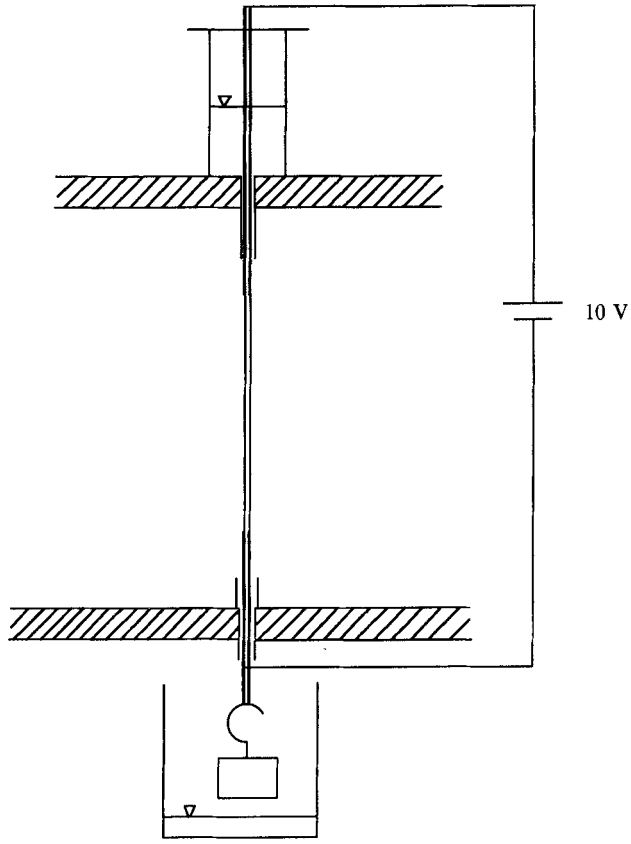

FIGURE 3. Side view of the smoke generator.

thicker copper wire with a diameter of 0.14 mm (figure 3). The reason for using two wires was that as an effect of system rotation the paraffin drops were thrown off the wire and this was eliminated with two wires. A light sheet illuminated the cross-flow plane at $x/d = 120$ where photographs were taken.

3. The effect of spanwise system rotation on primary instability

From hot-wire measurements it was possible to map the streamwise velocity field in a cross-section for different streamwise positions. The sampling time was typically 2 s which was sufficiently long when the vortices were stationary. In the following, hot-wire measurements together with smoke visualizations will be shown of the primary instability at $De = 70$ and five different rotation numbers at $x/d = 120$. Each measurement involved 61 points in the spanwise direction and 16 or 17 points in the radial direction. In the radial direction the step was 0.5 mm and in the spanwise direction 1 mm. A total of 17 cross-sections were measured for each rotation number.

In figure 4 photographs are shown of the smoke visualization, together with contour plots of the streamwise velocity and of the streamwise disturbance velocity. Here we define the latter as the measured velocity minus the spanwise average (from 61 points in the spanwise direction) of the measured velocity. The concave outer channel wall is at the top for each figure. Solid contour lines indicate positive disturbance velocity and the dashed lines show negative values. The zero contour lines are not plotted

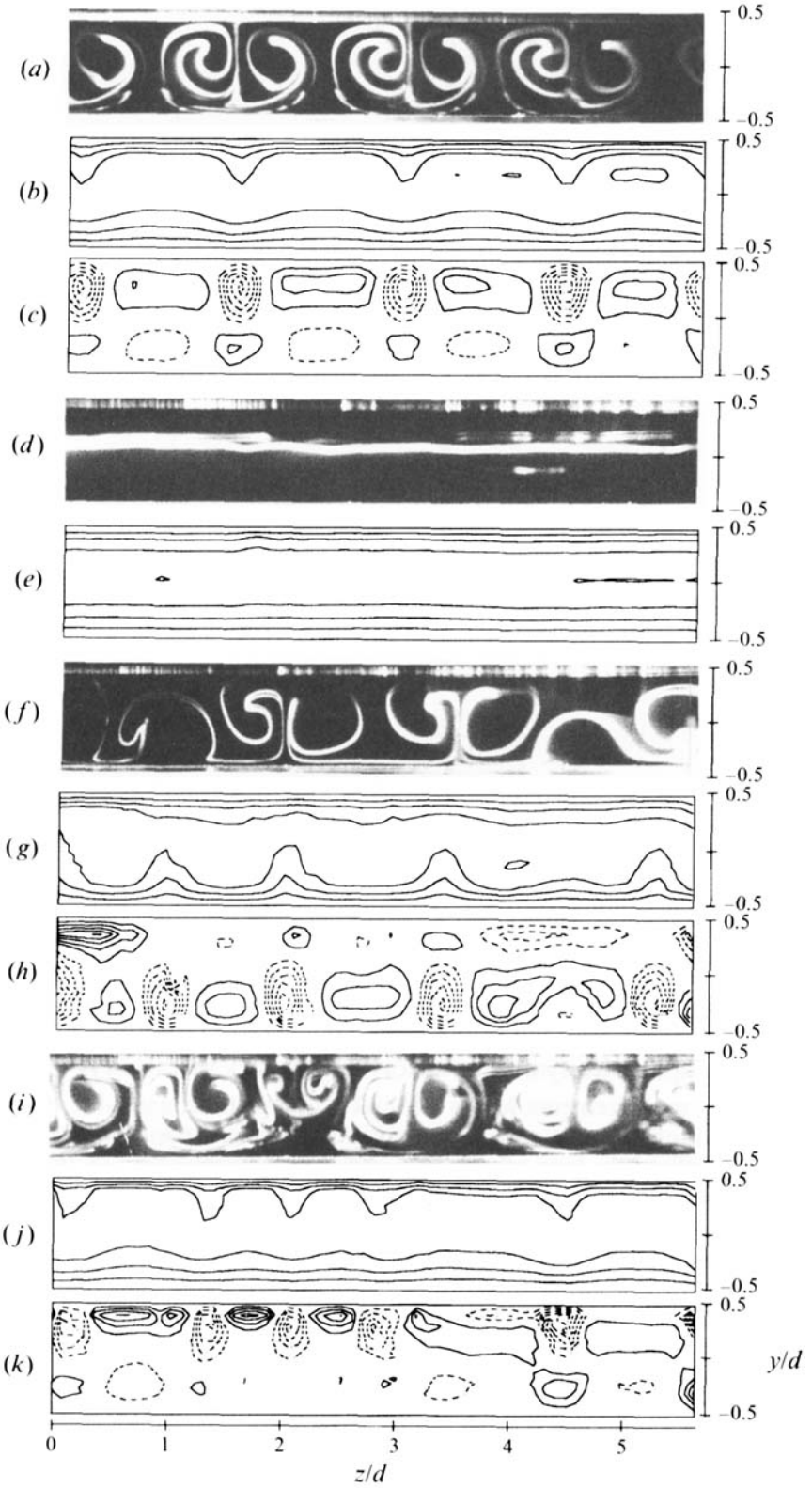

FIGURE 4. For caption see facing page.

in the figures. The triggered spanwise wavenumber ($\beta = 4.4$) can be compared with the spatially most amplified wavenumber ($\beta = 5.3$ at $De = 70$), obtained from linear stability theory. However, according to Guo & Finlay (1991) the wavenumber should be selected by the Eckhaus instability, which would give a value close to the triggered one.

Figure 4(*a*) shows a photograph in the cross-flow plane of the smoke visualization at $Ro = 0$. The smoke leaves the smoke wire as a sheet which is deformed by the streamwise vortices giving rise to a mushroom-shaped smoke pattern typical for the existence of Dean vortices. At this De the primary instability appeared as stationary longitudinal roll cells. The stem of the mushroom is an inflow region from the concave wall between a vortex pair. Figure 4(*b*) shows contour lines of the corresponding streamwise velocity. The waviness of the contour lines indicates the Dean vortices which move fluid at the concave wall with low streamwise velocity to the centre of the channel between vortex pairs, i.e. an inflow region from the concave wall. In the same way vortices move fluid with high streamwise velocity from the centre of the channel to the concave wall. Finally, contour lines of the streamwise disturbance velocity, u', are also shown for $Ro = 0$ in figure 4(*c*). Regions at the concave wall with negative streamwise disturbance velocity were squeezed in between the elongated positive disturbance regions.

In figure 4(*d*, *e*) a rotation number of $Ro = -0.03$ is shown to dramatically affect the flow and in the smoke visualization no vortices were visible. The smoke appeared as a white straight line in the middle of the channel, which was the position where the smoke wire was located further upstream. The contour lines of the streamwise velocity were parallel to the walls and accordingly the velocity profile was almost parabolic. A total disappearance of the vortices agreed with linear stability analysis which shows that for this Ro the flow should be stable for De below 150. However, at a higher rotation rate ($Ro = -0.05$, figure 4(*f*–*h*) the vortices appear again but for this case on the convex wall as it is the Coriolis force which dominates and give rise to the vortices.

For the other direction of rotation ($Ro = 0.03$) the Coriolis force enhanced the centrifugal force and the flow became less well-organized. It is evident that a new small vortex has appeared in figure 4(*i*–*k*) at $z/d \approx 2$ as a result of a splitting process which increased the spanwise wavenumber.

For $Ro = 0.05$ the smoke visualization showed a chaotic motion, but still vortices were visible. However, in the averaged streamwise velocity no vortices were distinguishable. This is probably because the vortices move randomly in the spanwise direction.

Spanwise-averaged radial profiles of the streamwise velocity were calculated in order to get a picture of how spanwise system rotation affects the mean streamwise

† The pattern to the right of each stem seems compressed in the spanwise direction compared to the pattern on the left side. The effect of gravity which acts from right to left is a possible explanation of this behaviour of the smoke.

‡ u' is defined as the velocity difference between the measured velocity at one specific y, z-position and the spanwise average of the streamwise velocity at the same y-position, $u'(y,z) = u(y,z) - (1/\Delta z)\int u(y,z)\mathrm{d}z$

FIGURE 4. Curved rotating channel flow for $De = 70$ at $x/d = 120$. Photographs of the smoke visualization, contour plots of the streamwise velocity (contour increment is $0.25U_{CL}$) and contour plots of the streamwise disturbance velocity (contour increment is $0.05U_{CL}$ and negative contours are dashed). (*a*–*c*) $Ro = 0$, (*d*, *e*) $Ro = -0.03$, (*f*–*h*) $Ro = -0.05$, (*i*–*k*) $Ro = 0.03$.

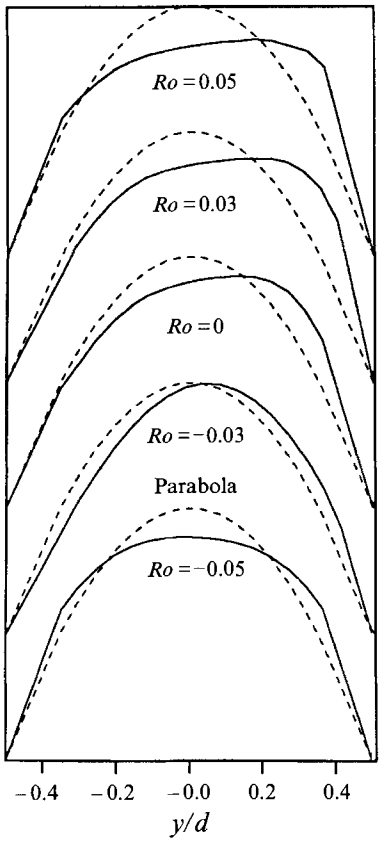

FIGURE 5. Spanwise-averaged profiles of the streamwise velocity for five different rotation numbers at $De = 70$.

velocity profile. In figure 5 these profiles are shown. For comparison the parabola is also shown in the same figure. The profiles for non-rotation and positive rotation have their maxima at the same radial position around $y/d = 0.2$. The profile for $Ro = -0.03$ resembled the parabola, with the same maximum level, but the radial position of the maximum was shifted slightly to $y/d = 0.05$. For $Ro = -0.05$ the profile was fairly symmetric around $y/d = 0$.

The streamwise development of the primary vortices subject to spanwise system rotation is an interesting feature that has also been explored in detail. Figures 6 to 8 show the streamwise development of the vortices without rotation and for the two negative rotation numbers shown in figure 4 at $De = 70$. In figure 6(a) ($Ro = 0$) contour plots of the streamwise disturbance velocity are shown at three different streamwise positions. In figure 6(a) the streamwise measuring position is located at $x/d = 60$ where the vortices were near their maximum amplitude. The inflow regions from the concave wall have an oval shape. Further downstream at $x/d = 90$ and $x/d = 120$, the amplitude of the inflow regions has decreased. Also the elongated positive regions near the concave wall became weaker.

In figure 7, $Ro = -0.03$, the streamwise velocity is shown instead of the streamwise disturbance velocity. The Coriolis force cancelled the Dean vortices at all three streamwise positions.

Increasing the rotation rate further to $Ro = -0.05$ gave a streamwise development

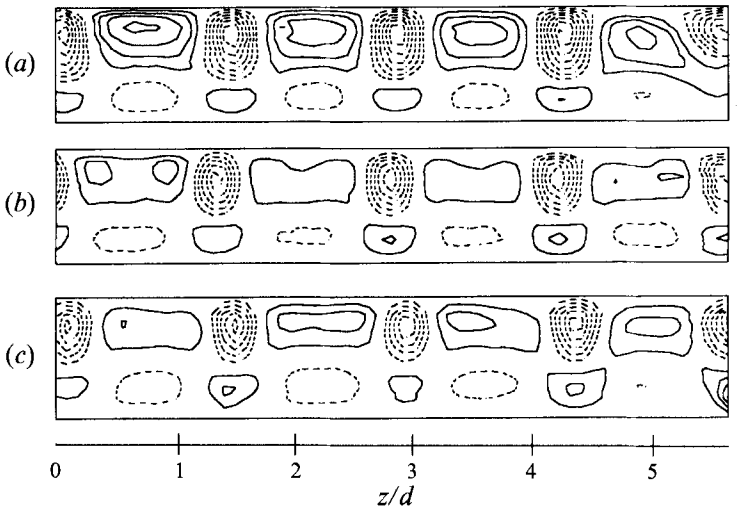

FIGURE 6. Streamwise development of curved channel flow for $De = 70$ at $Ro = 0$. Contour plots of the streamwise disturbance velocity (contour increment is $0.05U_{CL}$ and negative contours are dashed). (*a*) $x/d = 60$, (*b*) $x/d = 90$, (*c*) $x/d = 120$.

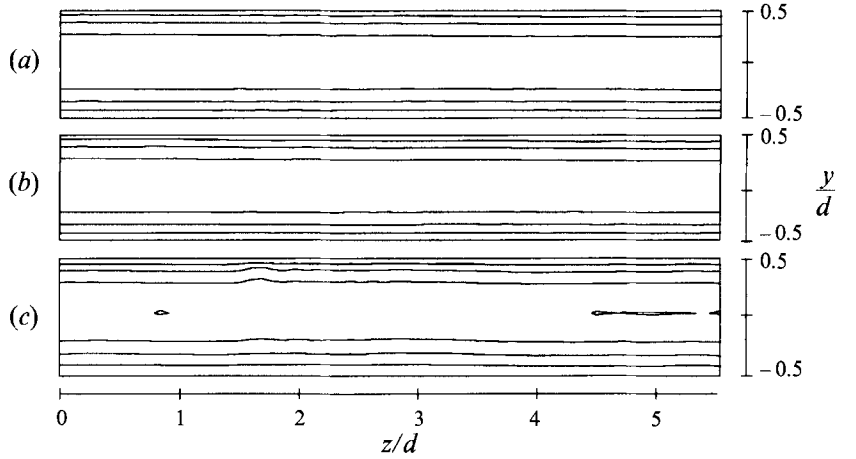

FIGURE 7. Streamwise development of curved rotating channel flow for $De = 70$ at $Ro = -0.03$. Contour plots of the streamwise velocity (contour increment is $0.25U_{CL}$). (*a*) $x/d = 60$, (*b*) $x/d = 90$, (*c*) $x/d = 120$.

as shown in figure 8. The vortices were located at the convex inner wall. Here it seems that a new vortex pair is formed around $z/d = 4.5$. The formation of vortices in between the triggered vortices is probably caused by an Eckhaus instability of the triggered vortices.

A measure of the strength of the vortices was obtained by evaluating the averaged streamwise disturbance amplitude in the measured cross-flow region as

$$e = \left(\frac{1}{A}\int u'^2 \mathrm{d}A\right)^{0.5},$$

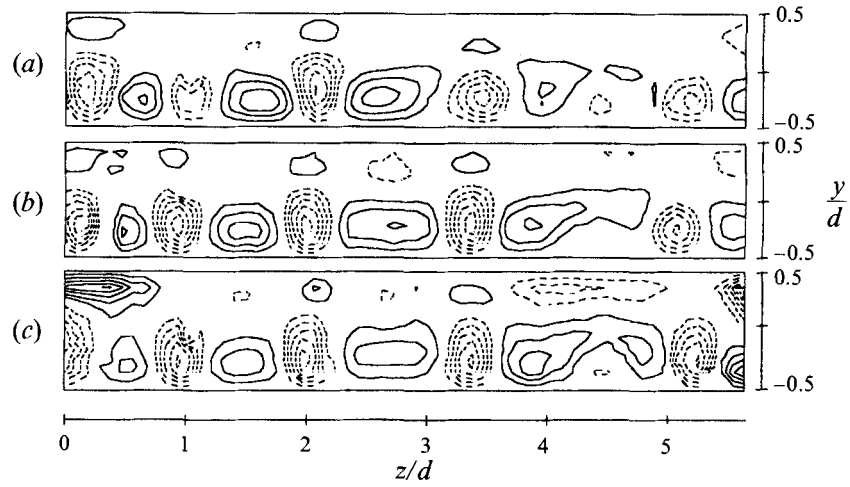

FIGURE 8. Streamwise development of curved rotating channel flow for $De = 70$ at $Ro = -0.05$. Contour plots of the streamwise disturbance velocity (contour increment is $0.05U_{CL}$ and negative contours are dashed). (*a*) $x/d = 60$, (*b*) $x/d = 90$, (*c*) $x/d = 120$.

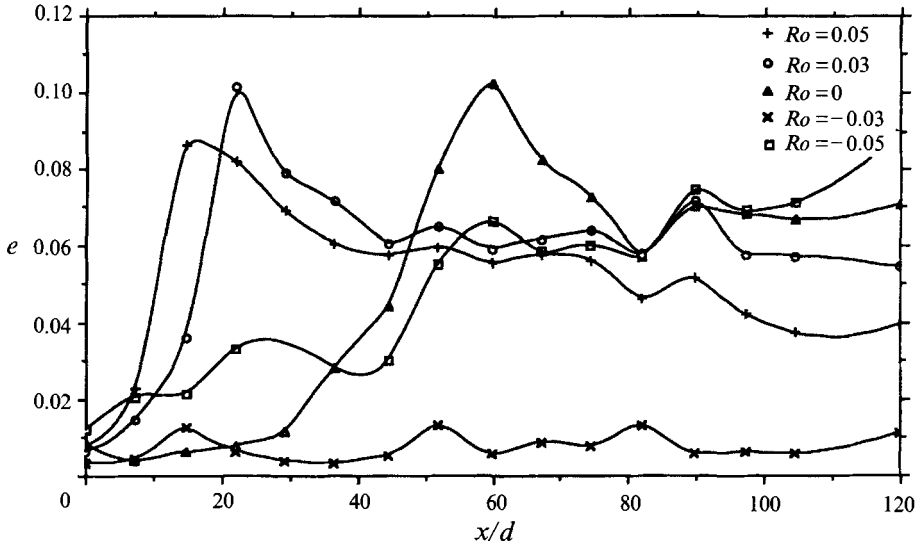

FIGURE 9. Streamwise development of the disturbance amplitude integrated over the measured part of the cross-flow plane for $De = 70$ at five different rotation numbers.

where A is the cross-sectional area of the integration. Figure 9 shows the disturbance amplitude of the vortices as function of the streamwise position. For $Ro = 0$ the amplitude increased downstream to a maximum ($e = 0.11$) at $x/d = 60$ and thereafter decreased to approximately $e = 0.07$. At $Ro = -0.03$, the amplitude was small and approximately constant ($e = 0.005$–0.01) along the channel, reflecting the fact that no vortices develop. That it is not exactly zero reflects the fact that the contour lines of the streamwise velocity are not perfectly parallel to the walls. On increasing the rotation rate to $Ro = -0.05$ the vortices appeared again and they contributed to a

growth of the amplitude in the streamwise direction, starting with a value of $e = 0.015$ at the start of curvature and reaching a maximum value of $e = 0.09$ at $x/d = 120$. For positive rotation numbers the maximum in amplitude moved closer to the start of curvature compared to the non-rotating flow situation. However, the levels of the maxima were close to that for non-rotation.

4. The effect of spanwise system rotation on secondary instability

Earlier measurements and simulations of curved channel flow have shown that secondary motions develop on top of the primary Dean vortices when De is increased. Three different types have been distinguished, and growth and interaction of these secondary instabilities will be a prelude to turbulent motion. One type of secondary instability is a travelling wave in the form of a so-called twisting motion in between the primary vortices. The second type of secondary instability is called undulating motion which is also of the travelling-wave type but having a longer wavelength than the twisting motion. The third type results in merging and splitting of the primary vortex pairs. In this section we will describe how spanwise system rotation affects these different types of secondary instabilities.

In the following, the streamwise development of the twisting and undulating motion will be shown without rotation and compared with positive and negative spanwise system rotation at $De = 162$. The measurements were taken around one vortex pair in the central part of the channel. Each measurement involved 34 points in the spanwise direction and 18 or 19 points in the radial direction. In both directions the increment of the measurements was 0.5 mm. The streamwise increment was 7.3 channel widths.

These measurements used time-resolved data in order to investigate the undulating and twisting instabilities separately. This was done by filtering the signals around the dominant frequency of the two instabilities. In this way it was possible to find the spatial extent of the two instabilities. The sampling time at each point was 20 s. It would have been desirable to use longer sampling times; however even with 20 s at each position the sampling time for each cross-section was approximately 4 hours†. The measured time sequence at each position was divided into five subsets on which FFT-analysis was done on-line to reduce the amount of data that needed to be stored. For the undulating motion the energy in the power spectrum was filtered around 10 Hz ($fd/U = 0.11$), but for the twisting motion the chosen frequency was dependent on the rotation number. The frequence was choosen such that the integrated r.m.s. distribution over the measured domain was a maximum. The filter width was 10 Hz for both the undulating and the twisting motion. In the following, the spatial distribution of the primary disturbance and the overall r.m.s. will be compared with that of the undulating and twisting motions.

In figures 10–12 results are shown for $Ro = 0$ at three different streamwise positions, namely $x/d = 75$, 97 and 120, where the twisting motion was obtained from the filtered signals with a centre-frequency of 100 Hz. Figure 10(a) shows contour lines of the streamwise disturbance velocity, which indicate a pair of counter-rotating streamwise vortices with the inflow region from the concave wall between a vortex pair. In figure 10(b), the total r.m.s. distribution is shown which has two local maxima near the concave channel wall where there are large spanwise gradients of the streamwise velocity. Figure 10(c) shows the high-frequency filtered part of the fluctuating signal

† In the following figures a weak 'smoothing' spatial filter has been used to reduce some of the irregularities due to too short averaging times.

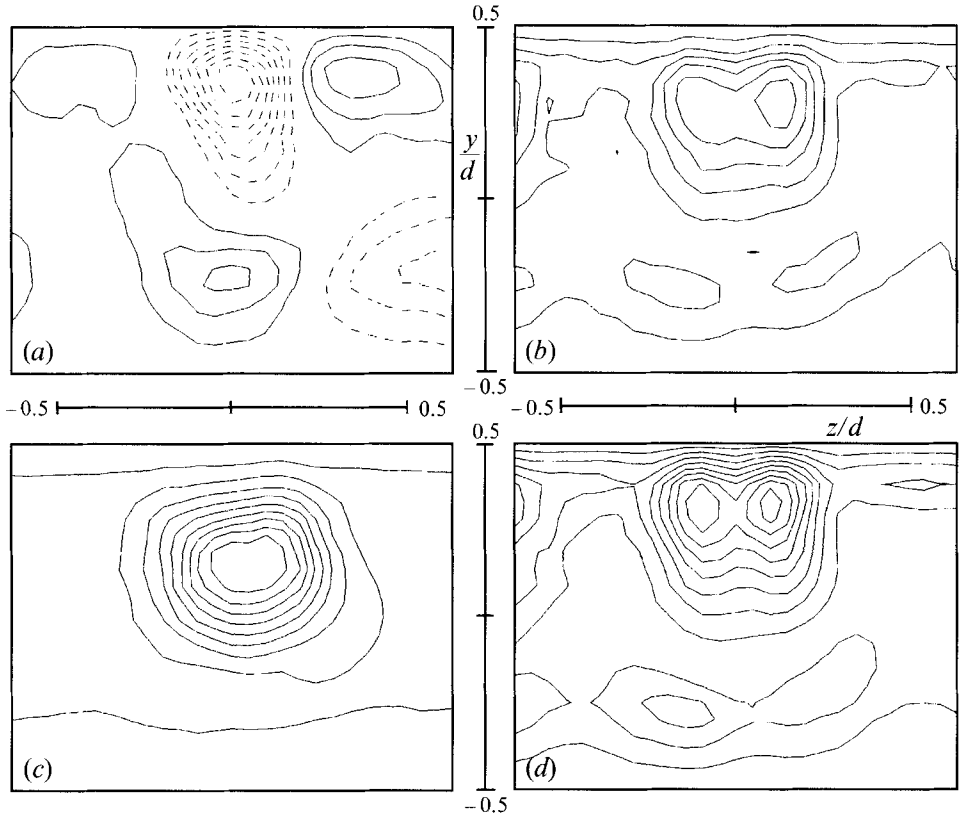

FIGURE 10. Curved rotating channel flow for $De = 162$ at $Ro = 0$, $x/d = 75$. (*a*) Streamwise disturbance velocity, i.e. the measured velocity minus the spanwise-averaged velocity profile (contour increment is $0.05U_{CL}$ and negative contours are dashed); (*b*) r.m.s. of streamwise velocity (contour increment is $0.01U_{CL}$); (*c*) r.m.s. levels for frequency band around twisting frequency (maximum level $0.0018U_{CL}$); (*d*) r.m.s. levels for frequency band around undulating frequency (maximum level $0.0430U_{CL}$). In (*c*) and (*d*) contours are 0.1, 0.2... of maximum level.

which shows that the secondary twisting motion appears in the low-velocity regions as pointed out by visual observations of the hot-wire signal, see Matsson & Alfredsson (1992). In this figure the contour lines show an almost circular shape of the domain where twists occur. Figure 10(*d*) shows contour lines of the undulating motion, which resembled the pattern of the r.m.s. distribution because the energy related to the undulating motion gives a large contribution to the total fluctuating energy. The increment between the contour lines for the twisting and undulating motion is chosen as one-tenth of the maximum value measured in the respective cross-section.

At $x/d = 97$ the amplitude of the twisting motion was at the maximum level. As seen in figure 11 the regions of the twisting and undulating motions were located closer to the concave channel wall and were more elongated in the spanwise direction compared to $x/d = 75$. This occurred in connection with an elongation of the inflow region between the primary vortex pair.

Figure 12 shows that the amplitude of the low-streamwise-velocity inflow region has decreased at $x/d = 120$. This may be an effect of the increased amplitude of the undulations which leads to a smearing out of the long-time-averaged primary

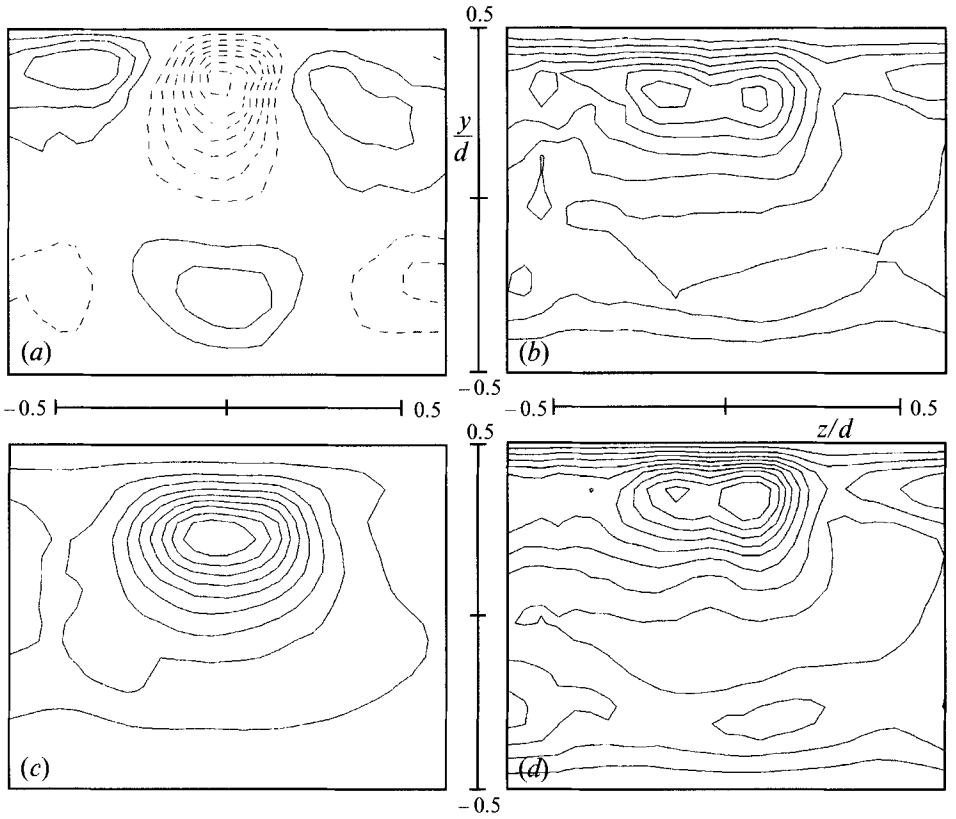

FIGURE 11. Curved rotating channel flow for $De = 162$ at $Ro = 0$, $x/d = 97$. (*a*) Streamwise disturbance velocity; (*b*) r.m.s. of streamwise velocity; (*c*) r.m.s. levels for frequency band around twisting frequency (maximum level $0.0077U_{CL}$); (*d*) r.m.s. levels for frequency band around undulating frequency (maximum level $0.0435U_{CL}$).

vortices. It can also be an effect of a merging between two vortex pairs. The low- and high-frequency regions were still clearly evident although they were also smeared out.

The secondary travelling wave instability may have one of two possible symmetries, usually called varicose and sinuous. For the streamwise velocity component, the varicose mode is symmetric and the sinous mode is antisymmetric in the spanwise direction around the inflow region from the concave wall. At first it was not clear whether the twisting motion was of sinuous or varicose type. In order to determine this a hot-wire probe was built with two wires positioned 2 mm apart in the spanwise direction and with the wires oriented radially in order to get a small extent in the spanwise direction. The wires were positioned symmetrically around an inflow region from the concave wall. Time signals of the voltage from the two wires are shown in figure 13. The signals are 180° out of phase, which would correspond to a sinuous mode of oscillation. This would indicate that the amplitude should be zero at the inflow symmetry line between a vortex pair. In contour plots of the twisting motion this should result in a minimum at the symmetry line which however is not apparent in figures 10–12. The reason for this may be that the undulation of the primary instability smeared out the two local maxima into one maximum in the middle between the local maxima. Some measurements of the distribution of

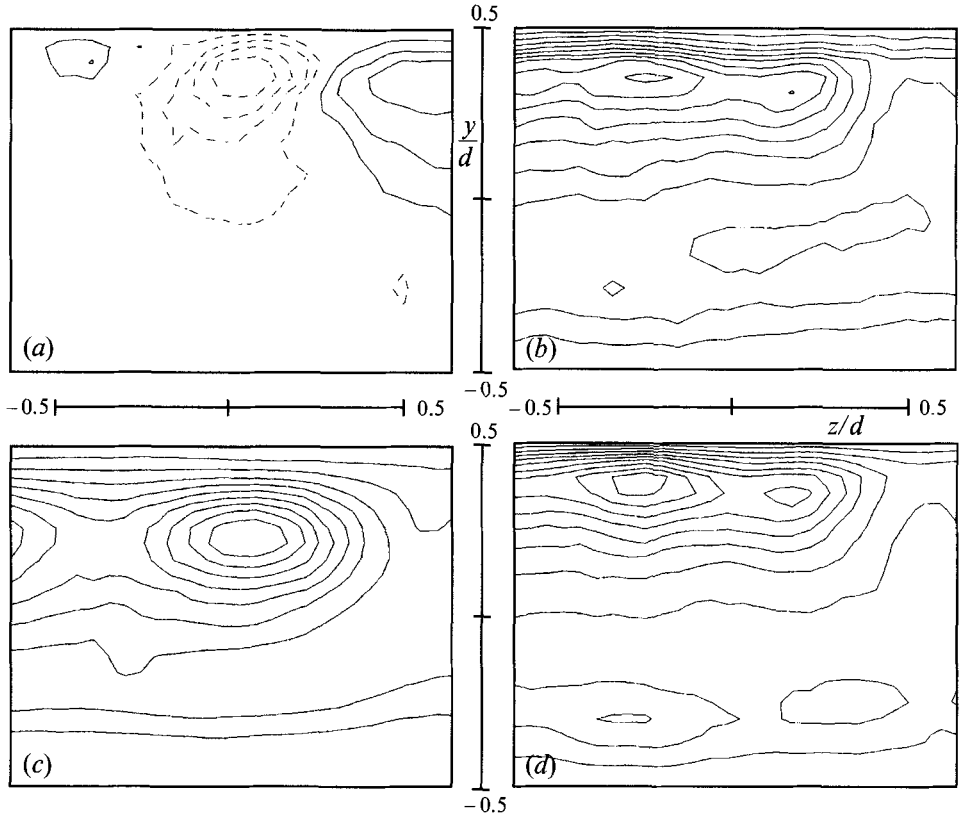

FIGURE 12. Curved rotating channel flow for $De = 162$ at $Ro = 0$, $x/d = 120$. (*a*) Streamwise disturbance velocity; (*b*) r.m.s. of streamwise velocity; (*c*) r.m.s. levels for frequency band around twisting frequency (maximum level $0.0061U_{CL}$); (*d*) r.m.s. levels for frequency band around undulating frequency (maximum level $0.0592U_{CL}$).

the twisting motion show two local maxima near the streamwise position where the twisting motion was first visible. At this position the primary vortices were probably more stable to undulations than further downstream.

Figures 14–16 show results obtained at a positive rotation number $Ro = 0.014$ at the same downstream positions as in the non-rotating case. The energy of the twisting motion was filtered around 100 Hz for all streamwise positions. Compared to the previous figures the physical twisting region was not as pronounced (at $x/d = 75$) as without system rotation. Furthermore, the two regions of local maxima for the undulation have merged and a prominent region of undulating motion was visible near the convex inner channel wall.

We also show similar data at $x/d = 120$ for a negative rotation number $Ro = -0.014$ in figure 17. For this case the energy of the twisting motion was filtered around 120 Hz. Here the amplitude of both the undulating and the twisting has dramatically decreased although the main features are the same. Notable is that the mean velocity field is similar to that at $x/d = 75$ for $Ro = 0$ but the amplitude of the secondary instability is smaller.

To get a clearer picture of the effect of rotation we have plotted the streamwise development of integral measures of (*a*) the amplitude of the primary instability, (*b*)

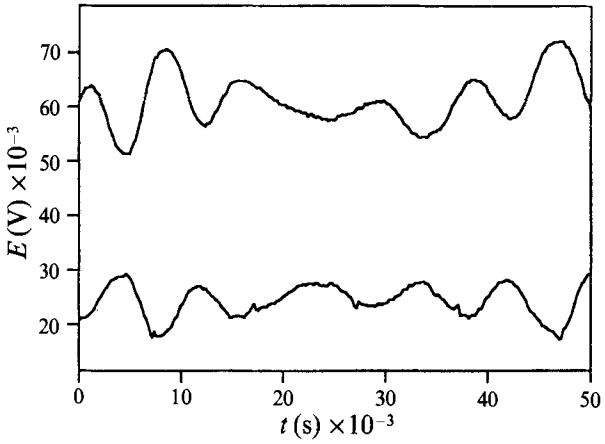

FIGURE 13. The time signal from two hot wires positioned symmetrically around an inflow region at $De = 162$, $Ro = 0$ and $x/d = 120$.

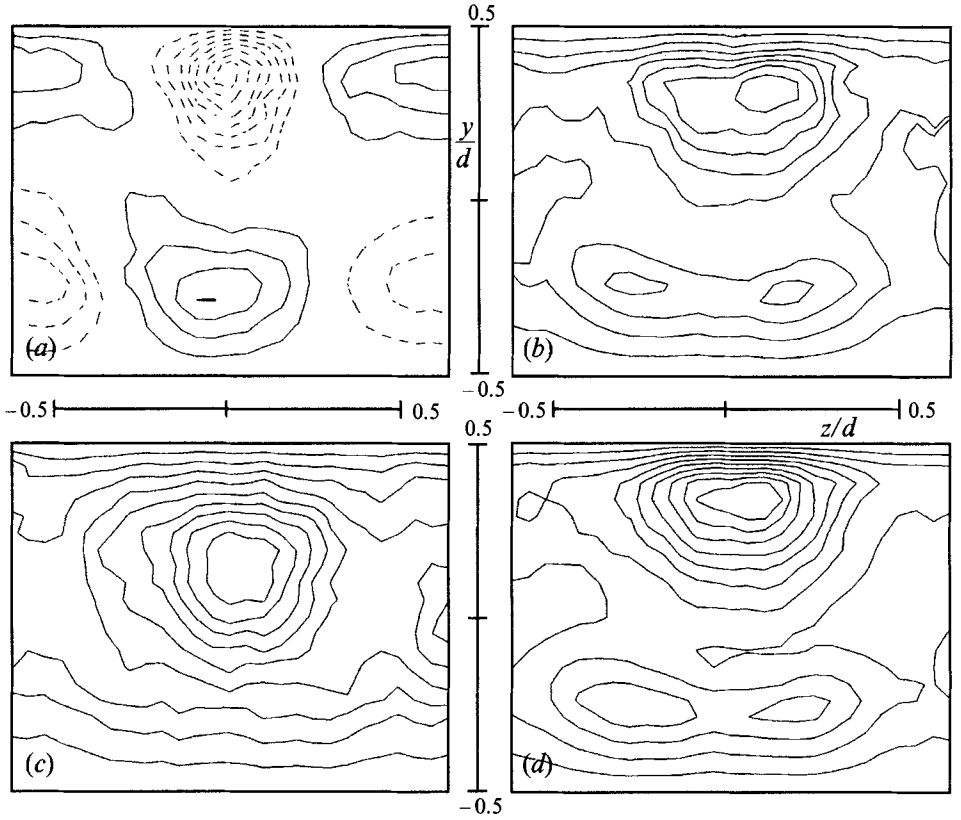

FIGURE 14. Curved rotating channel flow for $De = 162$ at $Ro = 0.014$, $x/d = 75$. (*a*) Streamwise disturbance velocity; (*b*) r.m.s. of streamwise velocity; (*c*) r.m.s. levels for frequency band around twisting frequency (maximum level $0.0017U_{CL}$); (*d*) r.m.s. levels for frequency band around undulating frequency (maximum level $0.0461U_{CL}$).

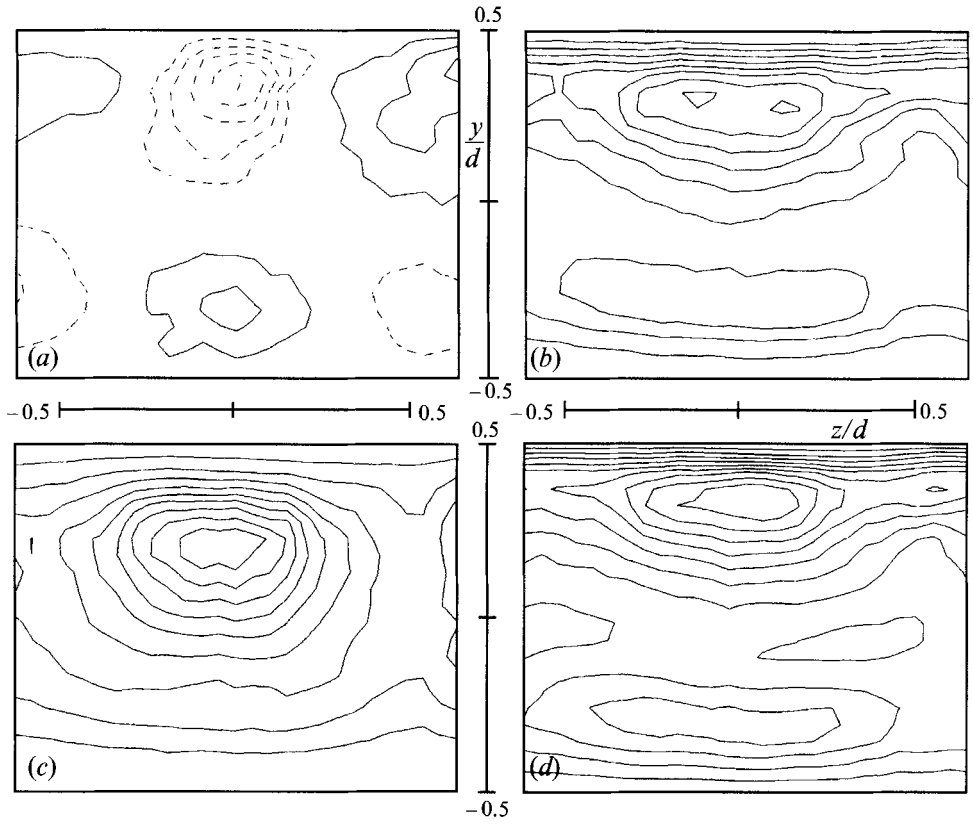

FIGURE 15. Curved rotating channel flow for $De = 162$ at $Ro = 0.014$, $x/d = 97$. (*a*) Streamwise disturbance velocity; (*b*) r.m.s. of streamwise velocity; (*c*) r.m.s. levels for frequency band around twisting frequency (maximum level $0.0048U_{CL}$); (*d*) r.m.s. levels for frequency band around undulating frequency (maximum level $0.0454U_{CL}$).

the total r.m.s. distribution, as well as (*c*) the twisting and (*d*) undulating secondary instabilities. Figure 18(*a*) shows the streamwise development of the averaged disturbance amplitude, e, for the three different rotation numbers $Ro = 0$, -0.014 and 0.014. The streamwise positions of the measurements were located downstream of the peak in the disturbance amplitude of the primary instability. The disturbance amplitude for $Ro = 0$ and $Ro = 0.014$ is lower than the amplitude for $Ro = -0.014$. The reason for this behaviour may be that the streamwise velocity field is more homogeneous in the spanwise direction for non-rotation and positive rotation compared to negative rotation. Figure 18(*b*) shows a measure of the integrated total r.m.s. distribution in the cross-flow plane defined as

$$\langle u_{rms} \rangle = \left(\frac{1}{A} \int u'_{rms}{}^2 \mathrm{d}A \right)^{0.5},$$

where u'_{rms} is the r.m.s. value of the measured velocity, which shows that positive rotation gives higher levels than non-rotation and negative rotation gives lower values compared to non-rotation. This result is in line with figure 18(*a*), i.e. positive rotation give rise to a higher overall r.m.s. level than non-rotation due to undulations which also leads to a more spanwise-homogeneous velocity field and thereby a lower

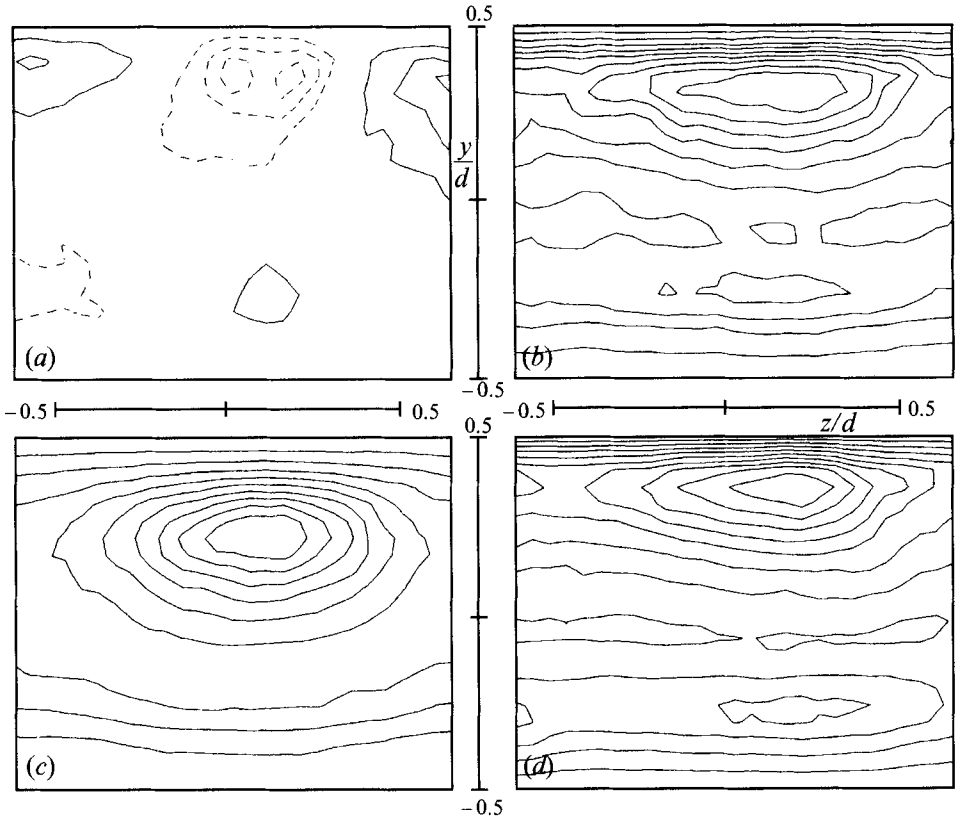

FIGURE 16. Curved rotating channel flow for $De = 162$ at $Ro = 0.014$, $x/d = 120$. (*a*) Streamwise disturbance velocity; (*b*) r.m.s. of streamwise velocity; (*c*) r.m.s. levels for frequency band around twisting frequency (maximum level $0.0061U_{CL}$); (*d*) r.m.s. levels for frequency band around undulating frequency (maximum level $0.0487U_{CL}$).

disturbance amplitude of the primary instability. Correspondingly, negative rotation decreases the r.m.s. level and causes a higher amplitude of the primary disturbance. Since the spanwise secondary instability is steady it will not affect the r.m.s. level. In figure 18(*c*), the integrated r.m.s. distribution for the filtered r.m.s. around the twisting frequency is shown. Without rotation, the amplitude increased exponentially to a certain, approximately constant, level. For the positive rotation number the growth of the secondary instability was almost the same as for non-rotation. For the negative rotation number the amplitude increased only at the streamwise positions furthest downstream and only to half the level for non-rotation and positive rotation. The corresponding integrated r.m.s. for the undulating motion and non-rotation was in between the levels for positive and negative rotation, see figure 18(*d*). However, at $x/d > 120$, the amplitude for non-rotation was higher than the corresponding amplitude for positive and negative spanwise system rotation.

5. Summary

The present experimental work shows for the first time experimentally obtained quantitative velocity data on the effects of spanwise system rotation on the primary

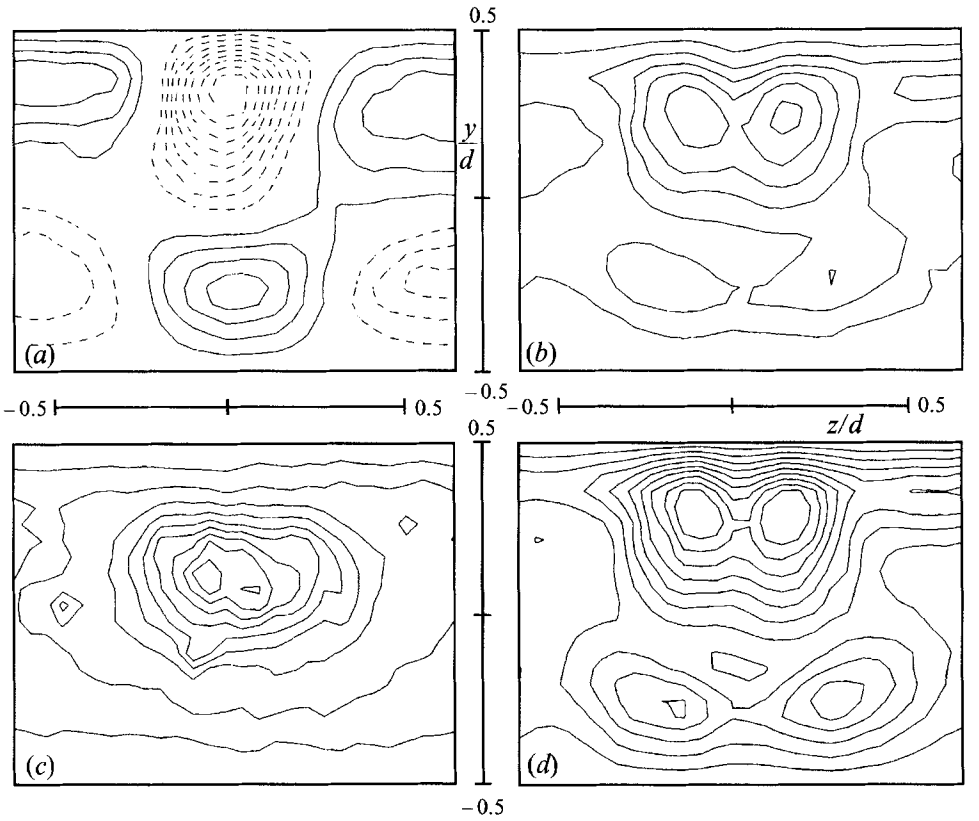

FIGURE 17. Curved rotating channel flow for $De = 162$ at $Ro = -0.014$, $x/d = 120$. (*a*) Streamwise disturbance velocity; (*b*) r.m.s. of streamwise velocity; (*c*) r.m.s. levels for frequency band around twisting frequency (maximum level $0.0018U_{CL}$); (*d*) r.m.s. levels for frequency band around undulating frequency (maximum level $0.0365U_{CL}$).

and secondary instabilities in curved channel flow. For curved channel flow at $De = 70$ the primary instability appears as steady vortices in the streamwise direction. Spanwise system rotation was shown to have a dramatic effect on the primary vortices. The Coriolis force was able to cancel the primary instability completely at $Ro = -0.03$, which was in excellent agreement with linear theory. Higher negative rotation gave rise to vortices on the convex inner channel wall. From flow visualizations in water by Matsson & Alfredsson (1990) it was shown in a streamwise–spanwise plane that the Coriolis force could cancel the primary instability for low rotation rates. In that experiment, the vortices reappeared at higher rotation rates, but it was not known at which side of the channel the vortices were located. However, in this paper it has been verified, by measurements and smoke visualization in a cross-flow plane, that the Coriolis force can give rise to vortices on the convex channel wall. For positive rotation, i.e. when the Coriolis force enhanced the centrifugal force, the flow became more unstable and splitting as well as merging of vortex pairs was observed. The spanwise wavenumber increases for positive rotation and decreases for negative rotation compared to non-rotation.

The measurements at $De = 162$ showed that the amplitude of the primary instability for the streamwise positions examined was higher for negative rotation than for non-

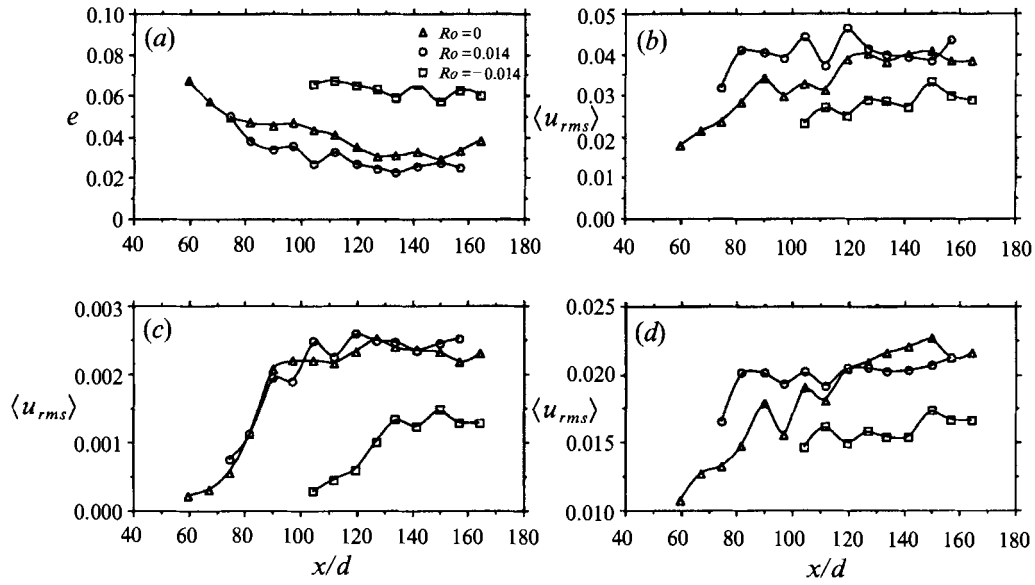

FIGURE 18. Amplitude growth in the streamwise direction. (*a*) Amplitude, *e*, of the averaged disturbance velocity; (*b*) r.m.s. of streamwise velocity; (*c*) filtered r.m.s. around twisting frequency; (*d*) filtered r.m.s. around undulating frequency. Results are shown for three different rotation numbers.

rotation and positive rotation. For non-rotating as well as rotating flow both twisting and undulating instabilities were found. The secondary twisting instability increased rapidly in amplitude in the streamwise direction up to a certain almost constant level. Spanwise system rotation in the negative direction reduced the amplitude of the secondary twisting instability. The frequency which gave rise to the highest integrated r.m.s. for the undulations was found to be 10 Hz and independent of rotation number. However, for the twisting motion the corresponding frequency was slightly higher for negative rotation and slightly lower for positive rotation compared with non-rotation.

From a preliminary secondary instability analysis following the lines of Ng *et al.* (1990) similar results were obtained as in the experiments. However, this analysis was made with the shape assumption, i.e. it uses the primary instability with a nonlinear amplitude and neglects the nonlinear distortion of the velocity distribution, which in this case is a crude approximation. In order to further resolve the issue one can study the linear stability of the measured profiles in the spanwise direction and the radial profiles in line with the work of Le Cunff & Bottaro (1993).

A complete picture of the secondary twisting and undulating motion is not yet fully developed. It is clear that inflectional profiles of the streamwise velocity in the spanwise direction are present. The experiments show that the undulating motion appears where these inflectional profiles are prominent and that the twisting motion appears where the streamwise disturbance velocity has its maximum negative value. The further development towards breakdown to turbulence remains to be investigated.

The financial support for this work from the Fluid dynamic research program of the National Board for Industrial and Technical Development (NUTEK) is gratefully acknowledged.

REFERENCES

ALFREDSSON, P. H. & PERSSON, H. 1989 Instabilities in channel flow with system rotation. *J. Fluid Mech.* **202**, 543–557.

ANDERECK, C. D., DICKMAN, R. & SWINNEY, H. L. 1983 New flows in a circular Couette system with co-rotating cylinders. *Phys Fluids* **26**, 1395–1401.

ANDERECK, C. D., LIU, S. S. & SWINNEY, H. L. 1986 Flow regimes in a circular Cuette system with independently rotating cylinders. *J. Fluid Mech.* **164**, 155–183.

AOUIDEF, A., WESFREID, J. E. & MUTABAZI, I. 1992 Coriolis effects on Görtler vortices in the boundary-layer flow on concave wall. *AIAA J.* **30**, 2779–2782.

BLAND, S. B. & FINLAY, W. H. 1991 Transitions toward turbulence in a curved channel. *Phys. Fluids* A **3**, 106–114.

BOTTARO, A. 1993 On longitudinal vortices in curved channel flow. *J. Fluid Mech.* **251**, 627–660.

BOTTARO, A., MATSSON, O. J. E. & ALFREDSSON, P. H. 1991 Numerical and experimental results for developing curved channel flow. *Phys. Fluids* A **3**, 1473–1476.

BREWSTER, D. B., GROSBERG, P. & NISSAN, A. H. 1959 The stability of viscous flow between horizontal concentric cylinders. *Proc. R. Soc. Lond.* A **251**, 76–91.

CHEN, F. & CHANG, M. H. 1992 Stability of Taylor–Dean flow in a small gap between rotating cylinders. *J. Fluid Mech.* **243**, 443–455.

CHENG, K. C., NAKAYAMA, J. & AKIYAMA, M. 1977 Effect of finite and infinite aspect ratios on flow patterns in curved rectangular channels. In *Flow visualization: Proc. Int Symp. on Flow Visualization, Tokyo* (ed. T. Asanuma), pp. 181–186.

DEAN, W. R. 1928 Fluid motion in a curved channel. *Proc. R. Soc. Lond.* A **121**, 402–420.

FINLAY, W. H., GUO, Y. & OLSEN, D. 1993 Inferring secondary flows from smoke or dye flow visualization: Two case studies. *Phys. Fluids* A **5**, 2689–2701.

FINLAY, W. H., KELLER, J. B. & FERZIGER, J. H. 1988 Instability and transition in curved channel flow. *J. Fluid Mech.* **194**, 417–456.

FINLAY, W. H. & NANDAKUMAR, K. 1990 Onset of two-dimensional cellular flow in finite curved channels of large aspect ratio. *Phys. Fluids* A **2**, 1163–1174.

GUO, Y. & FINLAY, W. H. 1991 Splitting, merging and wavelength selection of vortices in curved and/or rotating channel flow due to Eckhaus instability. *J. Fluid Mech.* **228**, 661–691.

GUO, Y. & FINLAY, W. H. 1994 Wavenumber selection and irregularity of spatially developing nonlinear Dean and Görtler vortices. *J. Fluid Mech.* **264**, 1–40.

KELLEHER, M. D., FLENTIE, D. L. & MCKEE, R. J. 1980 An experimental study of the secondary flow in a curved rectangular channel. *Trans. ASME* I: *J. Fluids Engng* **102**, 92–96.

LE CUNFF, C. & BOTTARO, A. 1993 Linear stability of shear profiles and relation to the secondary instability of the Dean flow. *Phys. Fluids* A **5**, 2161–2171.

LIGRANI, P. M., FINLAY, W. H., FIELDS, W. A., FUQUA, S. J. & SUBRAMANIAN, C. S. 1992 Features of wavy vortices in a curved channel from experimental and numerical studies. *Phys. Fluids* A **4**, 695–709.

LIGRANI, P. M. & NIVER, R. D. 1988 Flow visualization of Dean vortices in a curved channel with 40 to 1 aspect ratio. *Phys. Fluids* **31**, 3605–3617.

MASUDA, S. & MATSUBARA, M. 1989 Visual study of boundary layer transition on rotating flat plate. In *Laminar-Turbulent Transition* (ed. D. Arnal & R. Michel), pp. 465–474. Springer.

MATSSON, O. J. E. 1993 Time-dependent instabilities in curved rotating channel flow. *Phys. Fluids* A **5**, 1514–1516.

MATSSON, O. J. E. & ALFREDSSON, P. H. 1990 Curvature- and rotation-induced instabilities in channel flow. *J. Fluid Mech.* **210**, 537–563.

MATSSON, O. J. E. & ALFREDSSON, P. H. 1992 Experiments on instabilities in curved channel flow. *Phys. Fluids* A **4**, 1666–1676.

MATSSON, O. J. E. & ALFREDSSON, P. H. 1993 Secondary instability and breakdown to turbulence in curved channel flow. *Appl. Sci. Res.* **51**, 9–14.

MATSSON, O. J. E., BOTTARO, A. & ALFREDSSON, P. H. 1991 Transition to turbulence in curved channel flow. In *Eighth Symp. on Turbulent Shear Flows, Sept. 9-11, Münich, Germany*, Paper 18-2.

MATSUBARA, M. & MASUDA, S. 1990 Turbulent spots in a rotating Blasius boundary layer. In *Advances in Turbulence 3* (ed. A. V. Johansson & P. H. Alfredsson), pp. 204–210. Springer.

MUTABAZI, I., HEGSETH, J. J., ANDERECK, C. D. & WESFREID, J. E. 1988 Pattern formation in the flow between two horizontal coaxial cylinders with a partially filled gap. *Phys. Rev.* A **38**, 4752–4760.

MUTABAZI, I., NORMAND, C., PEERHOSSAINI, H. & WESFREID, J. E. 1989 Oscillatory modes in the flow between two horizontal corotating cylinders with a partially filled gap. *Phys. Rev.* A **39**, 763–771.

NG, L., SINGER, B. A., HENNINGSON, D. S. & ALFREDSSON, P. H. 1990 Instabilities in rotating channel flow. In *Instability and Transition*, vol. II (ed. M.Y. Hussaini & R.G. Voigt), pp. 313–329. Springer.

ZEBIB, A. & BOTTARO, A. 1993 Goertler vortices with system rotation: linear theory. *Phys. Fluids* A **5**, 1206–1210.